Fluid Phase Equilibria 436 (2017) 98–112

Contents lists available at ScienceDirect

Fluid Phase Equilibria

journal homepage: www.elsevier.com/locate/fluid

The spinodal of single- and multi-component fluids and its role in the development of modern equations of state

Peder Aursand [a], Magnus Aa. Gjennestad [a], Eskil Aursand [a, b], Morten Hammer [a], Øivind Wilhelmsen [a, c, *]

[a] SINTEF Energy Research, Sem Sælands vei 11, NO-7034 Trondheim, Norway
[b] NTNU, Department of Energy and Process Engineering, Kolbjørn Hejes vei 1B, NO-7491 Trondheim, Norway
[c] NTNU, Department of Electrical Engineering and Renewable Energy, Gunnerus Gate 1, NO-7491 Trondheim, Norway

ARTICLE INFO

Article history:
Received 24 October 2016
Received in revised form
7 December 2016
Accepted 19 December 2016
Available online 26 December 2016

Keywords:
Thermodynamics
Equation of state
Spinodal
Nucleation
Phase stability
Superheat limit

ABSTRACT

The spinodal represents the limit of thermodynamic stability of a homogeneous fluid. In this work, we present a robust methodology to obtain the spinodal of multicomponent fluids described even with the most sophisticated equations of state (EoS) available. We elaborate how information about the spinodal and its uncertainty can contribute both in the development of modern EoS and to estimate their uncertainty in the metastable regions. Inequality constraints are presented that can be exploited in the fitting of modern EoS of single-component fluids to avoid inadmissible pseudo-stable states between the vapor and liquid spinodals. We find that even cubic EoS violate some of these constraints.

With the use of a selection of EoS representative of modern applications, we compare vapor and liquid spinodal curves, superheat and supersaturation limits from classic nucleation theory (CNT), and available experimental data for the superheat limit. Computations are performed with pure species found in natural gas, binary mixtures, as well as a multi-component natural gas mixture in order to demonstrate the scalability of the approach. We demonstrate that there are large inconsistencies in predicted spinodals from a wide range of EoS such as cubic EoS, extended corresponding state EoS, SAFT and multiparameter EoS. The overall standard deviation in the prediction of the spinodal temperatures were 1.4 K and 2.7 K for single- and multi-component liquid-spinodals and 6.3 K and 26.9 K for single- and multi-component vapor spinodals.

The relationship between the measurable limit of superheat, or supersaturation, and the theoretical concept of the spinodal is discussed. While nucleation rates from CNT can deviate orders of magnitude from experiments, we find that the limit of superheat from experiments agree within 1.0 K and 2.4 K with predictions from CNT for single- and multi-component fluids respectively. We demonstrate that a large part of the metastable domain of the phase diagram is currently unavailable to experiments, in particular for metastable vapor. Novel techniques, experimental or with computational simulations, should be developed to characterize the thermodynamic properties in these regions, and to identify the thermodynamic states that define the spinodal.

1. Introduction

Metastable fluids can be found everywhere and continue to attract attention [1]. Recent examples include the ongoing discussion on cavitation of water at large negative pressures [2–6], magma erupting from volcanoes [7] and violent vapor-explosions from liquids spills in contact with a substantially warmer substance [8–11]. It is challenging to measure the properties of highly metastable fluids. By their own labile nature, they transform into a more stable phase via nucleation, where the nucleation process is triggered by thermal fluctuations. These fluctuations occur naturally, even in perfectly homogeneous fluids at equilibrium [12].

Properties of metastable fluids are central in the description of many processes. An important example is nucleation, which is ubiquitous in a wide range of physical, chemical, and biological processes. In nucleation theory, the thermodynamic state of the

* Corresponding author. SINTEF Energy Research, Sem Sælands vei 11, NO-7034 Trondheim, Norway.
E-mail address: oivind.wilhelmsen@ntnu.no (Ø. Wilhelmsen).

http://dx.doi.org/10.1016/j.fluid.2016.12.018

critical embryo is within the metastable region of the fluid [12]. Even for the simple case of condensation of the noble gas argon, predictions of nucleation rates from classical nucleation theory (CNT) deviate more than 20 orders of magnitude from experiments. In contrast, we will here show that CNT predicts accurately the "limit of superheat" for many hydrocarbons, which represents the experimentally available limit of metastability of liquids. Some of the deviation between several theories [13,14] and experimental data is likely because of inaccuracies in current equations of state (EoS) in the metastable regions [13].

In the development of modern multiparameter EoS, for example for water [15], the thermodynamic properties of metastable fluid phases such as subcooled liquid (metastable with respect to solid-liquid) and superheated liquid (metastable with respect to the vapor-liquid) are included in the fitting procedure. The extrema for metastability are defined by the spinodal. At the spinodal, the homogeneous fluid becomes intrinsically unstable and the activation barrier for nucleation disappears. The unstable fluid will then spontaneously decompose into the more stable phases. From a thermodynamic point of view, much is known about the state of the fluid at the spinodal. For instance, for single-component fluids, several thermodynamic properties such as the bulk modulus and the inverse isobaric heat capacity equal zero. Therefore, information about the spinodal is valuable, both in the development of modern EoS and to estimate their uncertainty in the metastable regions. Moreover, a thermodynamically consistent behavior of the EoS in the unstable domain of the homogeneous fluid is a prerequisite for combining them with mass based density functional theory for studying interfacial phenomena [16].

A major challenge in the study of metastable fluids is that there are limitations to how close to the spinodal one can get in experiments with real fluids. No matter how careful an experiment has been carried out, thermal fluctuations that occur naturally in the fluid will trigger homogeneous nucleation before the spinodal has been reached, even though the metastable domain extends significantly further. Highly metastable states that are experimentally unavailable for bulk fluids can still be encountered in small cavities, or within the critical cluster or cavity during nucleation, and are thus of practical relevance. The experimentally attainable limit where a superheated liquid spontaneously transforms into vapor is known as the *limit of superheat* [1]. The most popular experimental technique for measuring the limit of superheat is the droplet explosion method, a technique dating back to the early work of Wakeshima and Takata [17] and Moore [18]. The droplet explosion method remains the most popular technique to date [8,11], and represents one of the techniques that can bring the liquid closest to the spinodal [19]. We shall in this work discuss how close to the spinodal it is possible to get experimentally, and how to get even closer.

From a theoretical perspective, we shall elaborate how information about the spinodal and its uncertainty can contribute both in the development of modern EoS and to estimate their uncertainty in the metastable regions. With the use of a selection of EoS with varying degree of complexity, we predict the spinodal curves for pure species and mixtures. The predicted spinodals are compared to both the limit of superheated liquid and supersaturated vapor from CNT and available experimental data. The present paper extends previous work on the topic spanning the last three decades [9,20–24]. Whereas previous studies have focused on cubic EoS, where obtaining the spinodal curve is straightforward, we present a general and robust approach based on thermodynamic stability analysis. This allows us to calculate and compare spinodals from a number of EoS with very different functional forms and levels of complexity. Moreover, while previous works have focused mostly on pure species, we calculate spinodals for hydrocarbon mixtures with up to five components. We show that the functional form of the EoS can have a significant influence on the predicted spinodal.

2. Theory

In this section, we present the theoretical foundation for the work. We start in Sec. 2.1 by describing the different types of EoS that will be used. In Sec. 2.2, we discuss how the spinodal can be characterized, before we in Sec. 2.3 explain how to estimate the experimental limit of stability for a homogeneous fluid with classical nucleation theory.

2.1. Equations of state

2.1.1. Cubic EoS (PR, SRK)

The simplest type of EoS that can still predict the spinodal are the cubic EoS. These can in general be represented as

$$P = \frac{RT}{v-b} - \frac{a\alpha(T)}{(v-bm_1)(v-bm_2)}. \tag{1}$$

Here, P is the pressure, T is the temperature, R the universal gas constant, v the molar volume, and a, α, and b are parameters of the EoS. The constants m_1 and m_2 characterize various two-parameter cubic EoS. For instance, for the van der Waals (VdW) EoS, $m_1 = m_2 = 0$, for the Soave–Redlich–Kwong (SRK) EoS [25], $m_1 = 1$ and $m_2 = 0$, and for the Peng–Robinson (PR) EoS [26], $m_1 = -1 + \sqrt{2}$ and $m_2 = -1 - \sqrt{2}$. All these EoS are two-parameter cubic EoS in the sense that they use the two parameters a and b. For fluids with several components, mixing rules are used to compute the parameters a and b, which then depend on the composition.

2.1.2. Extended corresponding state EoS (SPUNG)

An extension of the corresponding state (CSP) methodology was initiated by Leach, Rowlinson and Watson as elaborated in Ref. [27], by including so-called "shape factors" that take into account how the mixture in consideration differs from the reference fluid(s). For pure components, this extension has a basis in statistical mechanics. If cubic EoS are used to calculate the shape factors, one may combine the strength of cubic EoS observed in VLE calculations with improved prediction of bulk properties obtained from a very accurate reference EoS. This methodology has also been referred to as the SPUNG EoS, and has proven to be both computationally fast as well as accurate [28]. We refer to Chapter 4 in Ref. [29] for further details.

2.1.3. Statistical associating fluid theory (SAFT)

Statistical Associating Fluid Theory (SAFT) gives EoS that are founded on statistical mechanics [30]. The perhaps most commonly used formulation is PC-SAFT [31] that has, in general, substantially improved accuracy in comparison with cubic EoS. Since PC-SAFT is founded on statistical mechanics and accounts for sizes and shapes of molecules, it is also expected to be the EoS with the largest predictive ability of the EoS considered in this work, in particular for polar substances and associating substances.

2.1.4. Multiparameter equations of state (GERG-2008)

Multiparameter EoS are today the most accurate EoS for the regions where thermodynamic property data are available. The EoS are founded on a comprehensive analysis of experimental data and a diligent optimization procedure, with functional forms optimized for accuracy. They have been devised for single-component fluids [15,32–36] and mixtures [37]. For some of these EoS, the thermodynamic properties of metastable fluid phases such as

supersaturated vapor and superheated liquid have been included in the fitting procedure [15]. In this work, we will use the multiparameter EoS for natural gas called GERG-2008 [37]. It is defined in terms of a reduced Helmholtz energy function:

$$\alpha(\rho,T,x) = \alpha^0(\rho,T,x) + \sum_{i=1}^{N_c} x_i \alpha_i^r(\rho,T) + \Delta\alpha^r(\rho,T,x), \tag{2}$$

where the superscripts 0 and r refer to the ideal gas and the residual contributions respectively, subscript i refers to species i, N_c is the number of components, ρ is the density and x_i is the mole fraction of component i. The last term on the right-hand-side, $\Delta\alpha^r$ is the departure function that takes into account the deviation from ideal mixture.

2.2. Thermodynamic stability and the spinodal

The spinodal represents the limit of intrinsic stability of a single-phase fluid. The spinodal is a theoretical limit, since thermal fluctuations will lead to homogeneous nucleation long before the spinodal has been reached in experiments, as explained in Sec. 1.

2.2.1. Thermodynamic stability in terms of the eigenvalues of the Hessian matrices of the energy state functions

Classical thermodynamics states that at equilibrium, the entropy of an isolated system is at its maximum. By considering an isolated composite system consisting of a subsystem that interacts with a thermal, pressure or particle reservoir, this criterion can be reformulated in terms of minima of various energy state functions for the subsystem [38]. The identity of the energy state function depends on the surroundings of the subsystem, or alternatively which state variables that have been fixed. Some examples are:

$$\min\{U(S,V,\mathbf{N})\} \quad \text{at fixed } S,V \text{ and } \mathbf{N} \tag{3}$$

$$\min\{A(T,V,\mathbf{N})\} \quad \text{at fixed } T,V \text{ and } \mathbf{N} \tag{4}$$

$$\min\{H(S,P,\mathbf{N})\} \quad \text{at fixed } S,P \text{ and } \mathbf{N} \tag{5}$$

$$\min\{G(T,P,\mathbf{N})\} \quad \text{at fixed } T,P \text{ and } \mathbf{N} \tag{6}$$

where U is the internal energy, A is the Helmholtz energy, H is the enthalpy, G is the Gibbs energy, S is the entropy, V is the total volume, and $\mathbf{N}$ is the mole numbers, where boldface symbols are vectors. In addition, in a single-component system, $U^* = U - N\mu$ is the Legendre transform of the internal energy with respect to the mole number, where μ is the chemical potential. Even if U^* is not commonly used in engineering applications, we shall refer to it in subsequent discussions. The energy state functions A, U^* and H are Legendre transforms of the internal energy with respect to one variable, while G is a Legendre transform of the internal energy with respect to two variables.

The thermodynamic stability of a stationary homogeneous system can be examined by evaluating the change in internal energy when decomposing into two phases, denoted with subscripts α and β (the initial system has no subscript). Let us start with an isolated system where U is a minimum at equilibrium, meaning that $\mathrm{d}U = \mathrm{d}(U_\alpha + U_\beta) = 0$, i.e. the system is in a *stationary* state. This condition implies uniform intensive variables: T, P and μ_i, where subscript i refers to component i (see Chapters 5 and 6 in Ref. [38]). However, a *stationary* state can be a minimum, maximum or saddle point. For the energy state function to be a minimum, the lowest order of non-vanishing variation must be positive. In most cases, this is the second order variation:

$$\mathrm{d}^2U = \mathrm{d}^2U_\alpha + \mathrm{d}^2U_\beta = \mathrm{d}\mathbf{x}_\alpha^T \ \nabla\nabla U_\alpha \ \mathrm{d}\mathbf{x}_\alpha + \mathrm{d}\mathbf{x}_\beta^T \ \nabla\nabla U_\beta \ \mathrm{d}\mathbf{x}_\beta \geq 0, \tag{7}$$

where $\mathrm{d}\mathbf{x}^T = [\mathrm{d}S, \mathrm{d}V, \mathrm{d}N_1, \ldots, \mathrm{d}N_{N_c}]$ represents an arbitrary change in the state variables and $\nabla\nabla U$ is the Hessian matrix of the internal energy, i.e. the matrix containing the second order partial derivatives of U with respect to the variables in $\mathbf{x}$. Since the system is isolated, $\mathrm{d}\mathbf{x}_\alpha = -\mathrm{d}\mathbf{x}_\beta$ and since the α and the β phases have uniform intensive variables, Eq. (7) can be reformulated as [39]:

$$\mathrm{d}\mathbf{x}^T \ \nabla\nabla U \ \mathrm{d}\mathbf{x} \geq 0, \tag{8}$$

where we have omitted subscript α and a scaling factor of N/N_β. Equation (8) can be rewritten in terms of the eigenvalues of $\nabla\nabla U$, λ_j:

$$\sum_{j=1}^{N_c+2} c_j^2 \lambda_j \geq 0, \tag{9}$$

where $\mathrm{d}\mathbf{x} = \sum_j^{N_c+2} c_j e_j$ and $e_1, \ldots, e_{N_c+2}$ are the eigenvectors of the Hessian matrix. Here, we have expressed the vector $\mathrm{d}\mathbf{x}$ in terms of the eigenvector-space of the Hessian matrix and the parameters, c_j, which can take any value. Since c_j^2 is always positive for any real number, the criterion for thermodynamic stability of an isolated system expressed by Eq. (7) can be reformulated as:

$$\min\{\mathrm{eig}(\nabla\nabla U)\} \geq 0, \tag{10}$$

i.e., the Hessian matrix of U should be positive-semidefinite. Legendre transforming the internal energy gives other energy state functions, and equivalent thermodynamic stability criteria can be formulated for these by following a similar approach as elaborated above:

$$\min\{\mathrm{eig}(\nabla_{V,\mathbf{N}}\nabla_{V,\mathbf{N}} \ A(T,V,\mathbf{N}))\} \geq 0 \quad \text{at fixed } T,V \text{ and } \mathbf{N} \tag{11}$$

$$\min\{\mathrm{eig}(\nabla_{S,\mathbf{N}}\nabla_{S,\mathbf{N}} \ H(S,P,\mathbf{N}))\} \geq 0 \quad \text{at fixed } S,P \text{ and } \mathbf{N} \tag{12}$$

$$\min\{\mathrm{eig}(\nabla_{\mathbf{N}}\nabla_{\mathbf{N}} \ G(T,P,\mathbf{N}))\} \geq 0 \quad \text{at fixed } T,P \text{ and } \mathbf{N} \tag{13}$$

where the subscripts indicate which variables are included in the del-operator, i.e. only the extensive variables of the respective potentials are included. In fact, at equilibrium, the Legendre transformed energy state functions are concave functions of their intensive canonical variables, and they are only a minimum if these variables are fixed [38] (see Eqs. (3)–(6)). The spinodal can thus be identified by investigating the eigenvalues of the Hessian matrices above. The criteria above are completely general, however, the typical textbook treatment defines an alternative way of identifying the spinodal in terms of a set of thermodynamic quantities that become zero at the spinodal. Since this method can give further insight, we shall discuss it next.

2.2.2. Thermodynamic stability in terms of selected thermodynamic derivatives

In conventional textbook literature on thermodynamic stability analysis, the approach outlined by Beegle et al. is often referred to [40], where the inner product between the Hessian matrices and $\mathrm{d}\mathbf{x}$ is examined in more detail. In particular, they show that some thermodynamic quantities go to zero before any other properties at the spinodal. In their textbook on classical thermodynamics, Tester and Modell state that a necessary and sufficient condition for thermodynamic stability is that [39]:

$$\frac{\partial^2 U^{(N_c)}}{\partial x_{N_c+1}\partial x_{N_c+1}} > 0, \tag{14}$$

where the superscript in $U^{(k)}$ denotes that the internal energy has been Legendre transformed with respect to the number k, of the first variables in the vector $\mathbf{x}^T = [S, V, N_1, \ldots, N_{N_c}]$. Moreover, x_l defines index l of the vector $\mathbf{x}$. The spinodal is then defined in terms of the following equation:

$$\frac{\partial^2 U^{(N_c)}}{\partial x_{N_c+1}\partial x_{N_c+1}} = 0. \tag{15}$$

However, the order of the variables in $\mathbf{x}$ can be chosen arbitrarily. Therefore, Eq. (15) results in several thermodynamic identities that equal zero at the spinodal. For a single-component system, these are:

$$\frac{\partial^2 A}{\partial x_k^2} : -\left(\frac{\partial P}{\partial V}\right)_{T,N} = 0 \quad \text{and} \quad \left(\frac{\partial \mu}{\partial N}\right)_{T,V} = 0 \tag{16}$$

$$\frac{\partial^2 U^*}{\partial x_k^2} : \left(\frac{\partial T}{\partial S}\right)_{\mu,V} = 0 \quad \text{and} \quad -\left(\frac{\partial P}{\partial V}\right)_{\mu,S} = 0 \tag{17}$$

$$\frac{\partial^2 H}{\partial x_k^2} : \left(\frac{\partial \mu}{\partial N}\right)_{P,S} = 0 \quad \text{and} \quad \left(\frac{\partial T}{\partial S}\right)_{P,N} = 0 \tag{18}$$

where Eq. (16) contains the diagonal entries of $\nabla_{V,N}\nabla_{V,N}$ A, Eq. (17) of $\nabla_{S,V}\nabla_{S,V}$ U^* and Eq. (18) of $\nabla_{S,N}\nabla_{S,N}$ H. All of these equations are satisfied simultaneously at the spinodal, where they change from positive to negative. An interesting question we shall discuss in Sec. 3.1 is whether the left-hand-side of Eqs. (16)–(18) should remain negative between the vapor and liquid spinodals. Such information is useful in the development of modern EoS, because if one can argue that thermodynamic quantities such as those defined in Eqs. (16)–(18) should remain negative, they can be exploited as inequality constraints in the fitting of single-component EoS to avoid inadmissible pseudo-stable states between the vapor and liquid spinodals. Any of the thermodynamic quantities in Eqs. (16)–(18) can be used equivalently to locate the spinodal of a single-component fluid.

2.2.3. The numerical algorithm used to identify the spinodal in this work

The Hessian matrices of all the energy state functions are singular, i.e. one of their eigenvalues is always zero. The reason for this is that the energy state functions are Euler homogeneous functions of first degree with respect to their extensive variables, while the Hessian matrices contain derivatives of only intensive variables (see Theorem 4, Chapter 1 in Ref. [41]). In practice, the spinodal can be found by eliminating one row and one column of the Hessian matrix of an appropriate energy state function to construct the matrix Φ. In the stable domain, Φ is non-singular, and the smallest eigenvalue becomes 0 at the spinodal (see Theorem 6, Chapter 1 in Ref. [41]). In this work, we have used the following criterion to identify the spinodal:

$$\min\{\mathrm{eig}(\Phi)\} = 0 \quad \text{where} \quad \Phi = \nabla_{\mathbf{N}}\nabla_{\mathbf{N}} A(T, V, \mathbf{N}). \tag{19}$$

The use of the Helmholtz energy formulation has proven numerically robust when solving for critical points [42]. Applying the Hessian scaling suggested by Michelsen [43], the spinodal is found by solving for the temperature at a given specific volume. A second-order method that uses numerical differentials for the minimum eigenvalue, $\lambda_{\min}$ is used. The eigenvalue calculation of a symmetric matrix can be performed with high numerical efficiency. With a given initial point on the spinodal, the entire spinodal curve can easily be traversed with the use of uniform steps in $\ln(V)$. Extrapolation from a known spinodal point can be achieved by utilizing:

$$\mathrm{d}\lambda_{\min} = \left(\frac{\partial \lambda_{\min}}{\partial T}\right)_V \mathrm{d}T + \left(\frac{\partial \lambda_{\min}}{\partial V}\right)_T \mathrm{d}V = 0, \tag{20}$$

which provides a good initial value for the temperature at the next spinodal point.

2.3. The experimentally available limit of stability of a homogeneous fluid as predicted by classical nucleation theory (CNT)

When a liquid has been sufficiently superheated, the homogeneous nucleation rate becomes at some point so large that the liquid transforms into two phases in a much shorter time than the characteristic time of the experiment. This corresponds to the observed superheat limit, and nucleation theory can thus be used to predict this.

Nucleation is an activated process where an energy barrier must be overcome by thermal fluctuations. Accordingly, the nucleation rate J depends exponentially on the height of the nucleation barrier according to a standard Arrhenius rate law,

$$J = K\exp\left(-\frac{\Delta G^*}{k_B T}\right), \tag{21}$$

where ΔG^* is the nucleation barrier, k_B is Boltzmann's constant, and K is the kinetic prefactor. Equation (21) can be used both to describe the formation of bubbles and droplets; however, the expression for K and ΔG^* differ in the two cases. The nucleation barrier, ΔG^*, is:

$$\Delta G^* = \frac{4\pi\sigma r^{*2}}{3}, \tag{22}$$

where the radius of the critical cluster or cavity r^*, for bubble formation in a liquid [1], is

$$r^* = \frac{2\sigma}{P_{\mathrm{sat}}(T) - P_{\mathrm{l}}}, \tag{23}$$

or for droplet formation in a gas [1],

$$r^* = \frac{2\sigma}{\tilde{\rho}_{\mathrm{l}} k_B T \ln(P_{\mathrm{g}}/P_{\mathrm{sat}})}, \tag{24}$$

where $\tilde{\rho}_{\mathrm{l}}$ is the number density of the liquid phase. Further, the kinetic prefactors can be approximated by following a range of approaches. In this work, we have used the following expressions to calculate the kinetic prefactor for bubble formation in a liquid [1]:

$$K \approx \tilde{\rho}_{\mathrm{l}}\sqrt{\frac{2\sigma}{\pi m}}, \tag{25}$$

where $\tilde{\rho}_{\mathrm{l}}$ is the number density of the liquid phase and m is the mass of one molecule. For droplet formation in a gas, we have used [1]:

$$K \approx \frac{\tilde{\rho}_{\mathrm{g}}^2}{\tilde{\rho}_{\mathrm{l}}}\sqrt{\frac{2\sigma}{\pi m}}, \tag{26}$$

where $\tilde{\rho}_{\mathrm{g}}$ is the number density of the vapor-phase, i.e. Eqs. (25) and (26) differ by the factor $(\tilde{\rho}_{\mathrm{g}}/\tilde{\rho}_{\mathrm{l}})^2$. We have in this work provided only

the necessary formulas, and we refer to Refs. [1,44] for details and derivations. Once the nucleation barrier has been found and the kinetic prefactors have been estimated based on properties at saturation, the nucleation rate can be calculated by use of Eq. (21). However, to set a specific limit of superheat or supersaturation, one must decide on a *critical* nucleation rate that represents the observed sudden phase change. Experiments indicate values of J_{crit} in the range $10^2 - 10^6$ cm^{-3} s^{-1} [1]. Since the exact value of the critical nucleation rate has very little influence on the predicted limit of superheat (See Fig. 3.13 in Ref. [1]) we use $J_{\text{crit}} = 10^6$ cm^{-3} s^{-1} in this work.

Given a value for J_{crit}, we find the superheat/supersaturation temperature limits for a given pressure and composition by solving

$$J(T) = J_{\text{crit}}, \tag{27}$$

for T. In order to complete this model, thermodynamic properties are needed. The pressures and densities are supplied by an EoS, and in this work we have used the most accurate EoS for the components in natural gas, GERG2008 [37]. Pure component surface tensions were modeled by the corresponding state correlation recommended in Ref. [45] (see Chapter 12). The deviation between this correlation and experiments is below 5% for most fluids according to Tables 12–1 in Ref. [45]. The procedure for finding the limits of superheat/supersaturation is described above for pure components. We extend it to mixtures by replacing the saturation properties by the properties at the bubble line (superheat limit) or at the dew line (subcool limit) of the mixture. The molecule mass m is then replaced by the mole fraction averaged molecule mass. Also, we use the mole fraction weighted average of the pure component surface tensions.

3. Results

We shall in Secs. 3.1 and 3.2 discuss the vapor and liquid spinodals from a theoretical perspective and their relevance in the development of EoS. Next, we evaluate in Sec. 3.3 how much the spinodals predicted from various EoS differ, and the implications of this on prediction of properties in the metastable regions. Eventually, we discuss in Sec. 3.4 how close to the spinodal that current experiments can bring us. In the following, we will focus on hydrocarbons and their mixtures.

3.1. The spinodals and their relevance for developing EoS

Properties of metastable fluids have received much attention in recent literature, partly because such states are ubiquitous in nature, including in important processes such as nucleation of droplets or bubbles in condensation and evaporation processes. It is therefore important to develop EoS that give an accurate representation of the metastable regions of the fluid.

Fig. 1a shows the pressure as a function of the density for methane at $T = 175$ K, as predicted by the Peng–Robinson cubic EoS. The figure highlights five regimes, one regime with single-phase gas at low densities (green solid line), one regime with single-phase liquid at high densities (blue solid line), two regimes where the single-phase fluid is metastable (dashed lines) and one regime where it is unstable (dotted line). If the inequality, $(\partial P/\partial \rho) < 0$, is satisfied where ρ is the density (equivalent to Eq. (16)-left), the single-phase fluid is mechanically unstable and will spontaneously decompose into liquid and vapor.

The shape of the pressure, P plotted as a function of the density, ρ displayed in Fig. 1a with a local maximum followed by a local minimum is called a Maxwell loop. Many EoS have a single Maxwell loop, but some EoS have a second, artificial Maxwell loop in the two-phase region. One example is shown in Fig. 1b, where GERG2008 (blue solid line) exhibits a second loop. Since $(\partial P/\partial \rho) > 0$ (mechanically stable) and also other thermodynamic stability criteria are satisfied, the EoS predicts a pseudo-stable single-phase fluid within a region where experiments show a coexistence between vapor and liquid. For many fluids and conditions, the pseudo-stable phase has even a lower energy than the vapor-liquid coexistence [16]. The second Maxwell loop is an artifact of the functional form and parameters of the GERG2008 EoS, and is a general problem/challenge in the present development of multiparameter EoS.

Fig. 1b shows the behavior of several EoS in the metastable and unstable regions, and elucidates some important points:

- The exact location of the spinodals (the maxima and minima) varies much with the choice of EoS.
- The EoS have different behaviors between the spinodals; some EoS exhibit a thermodynamically consistent behavior (a single Maxwell loop), while other EoS do not.
- The behavior of the metastable regions depends much on the choice of EoS.

A goal should be to develop EoS that are accurate and thermodynamically consistent, also in the metastable and unstable regions of the phase diagram of the single-phase fluid. A future goal should be to develop EoS without inadmissible pseudo-stable states in the unstable domain of the single-phase fluid. This is of importance, both for combining them with mass based density functional theory and to develop thermodynamically consistent mixing rules with a physical interpretation as elaborated in detail in Ref. [16].

Fig. 1b shows that GERG2008 and PC-SAFT follow each other closely in the first part of the metastable regions. This is expected, as their Taylor-expansions of the pressure as a function of density about the saturation state are very similar, because they both reproduce well the thermodynamic properties at saturation from experiments. Therefore, accurate prediction of equilibrium properties at the saturation curve is a prerequisite for accurately predicting properties in the metastable regions. However, the figure also shows that GERG2008 and PC-SAFT predict very different pressures for the onset of the liquid-spinodal (the minima of the curves). Since equilibrium measurements at saturation can provide the right slope of, for instance P as a function of ρ into the metastable regions, the location of the spinodal would provide a reference for this extrapolation. Therefore, if it was possible to find the precise onset of the spinodal, either through experiments or computations, it would be possible to characterize the whole metastable region with good accuracy. Moreover, if the spinodal could be determined to some degree of uncertainty it would be possible, based on the known uncertainty of properties at coexistence, to make statements about how accurate extrapolations to the metastable regions from various EoS are. We shall discuss the current uncertainty in the prediction of the liquid and vapor spinodals in Sec. 3.3.

One of the more urgent challenges in the development of EoS is to remove the second artificial Maxwell loop in the two-phase region, an artifact characteristic for so-called multiparameter EoS (see Sec. 2.1.4). Multiparameter EoS are founded on a comprehensive analysis of experimental data and a diligent optimization procedure, with functional forms optimized for accuracy. By adding new terms to the Helmholtz energy functional of multiparameter EoS and with the use of additional constraints in the nonlinear fitting routine, Lemmon and Jacobsen managed to reduce the magnitude of the second Maxwell loop in the multiparameter EoS for the fluid R125 [46] from $\sim 10^6$ MPa to below $\sim 10^2$ MPa. In 2009, Lemmon et al. presented a multiparameter EoS for propane,

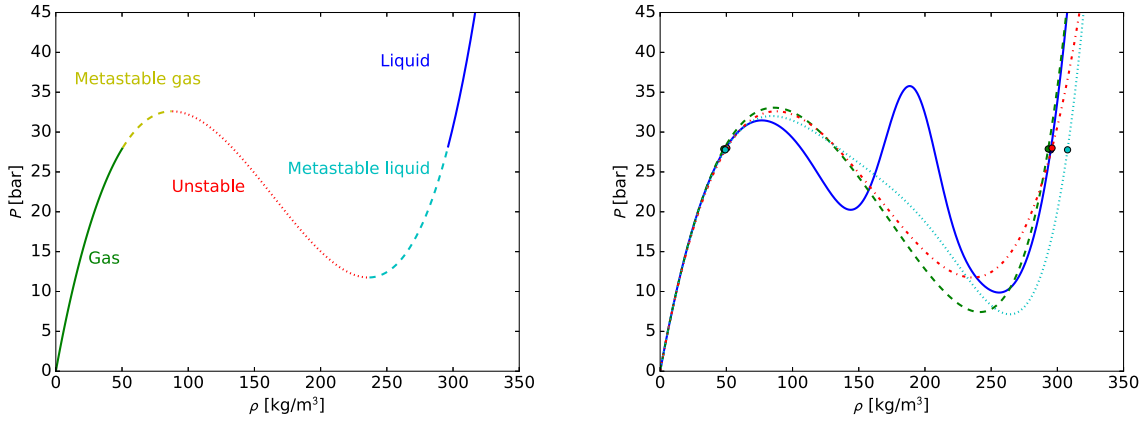

Fig. 1. Pure methane isotherms at 175 K. (a), the stable, metastable and unstable regions are illustrated by an isotherm as predicted by the PR EoS. (b), isotherms are drawn with different EoS: GERG2008 (solid blue), PC-SAFT (dashed green), PR (dash-dot red) and extended CSP (dotted cyan). The saturation points are indicated by circles. (For interpretation of the references to colour in this figure legend, the reader is referred to the web version of this article.)

where they reverted back to the functional form with Gaussian bell shaped terms [47]. With the use of the new fitting techniques and constraints from Ref. [46], they were able to reduce the magnitude of the artificial Maxwell loop. Recent multiparameter EoS are formulated with the functional form presented in Ref. [47]. Lemmon and Jacobsen implemented the constraint discussed by Elhassan et al. [48]:

$$a(\rho) - a_{\text{tang}}(\rho) \geq 0 \tag{28}$$

where a is the Helmholtz energy and subscript tang means the Helmholtz energy evaluated at the equilibrium tangent line. Despite what Elhassan and coauthors claim in their work [48], the constraint in Eq. (28) does not "remove any inconsistencies between thermodynamic stability and physical reality". Even if Eq. (28) guarantees that both the Helmholtz energy and the Gibbs energy of the vapor-liquid coexistence state is lower than the Gibbs energy of a pseudo-stable state coming from a second Maxwell loop [48], the pseudo-stable state can still be stable in other ensembles such as in an isolated system. We have elaborated in detail on this in Ref. [16].

3.2. Inequality constraints to avoid inadmissible pseudo-stable states between the spinodals

Since the inequality in Eq. (28) is insufficient for constraining EoS to avoid inadmissible pseudo-stable states in the unstable-region of the single-phase fluid (between the spinodals), we shall next discuss which inequality constraints that can be used instead. The derivatives in Eqs. (16–18) are natural candidates for such inequality constraints for the single-component fluid, since they reach zero before any other thermodynamic identities at the spinodals. We note that similar thermodynamic quantities can be defined for multicomponent fluids [39], and exploited in the fitting of multiparameter EoS for mixtures, such as GERG2008. We shall now evaluate Eqs. (16–18) for an EoS that is considered, from a qualitative perspective, to have a physically admissible behavior in the two-phase region: the Van der Waals cubic (VdW) EoS.

Fig. 2 plots Eqs. (16–18) for methane at 92 K through the metastable and unstable regions of the single-phase fluid, as predicted by the VdW EoS. The figure shows that all six of the thermodynamic quantities in Eqs. (16–18) reach zero at exactly the same two densities ($\rho = 32$ kg/m^3 and $\rho = 251$ kg/m^3), as shown by the vertical red dashed lines. These two densities define the vapor and liquid spinodals. At constant temperature, these are the only two densities where the thermodynamic quantities in Eqs. (16–18) equal zero.

If we examine the sign of the thermodynamic relations in Eqs. (16) and (18), only four of them remain negative between the vapor and liquid spinodals (vertical red dashed lines). The two thermodynamic relations that represent the diagonal entries of the Hessian matrix of the enthalpy, $(\partial\mu/\partial N)_{P,S}$ and $(\partial T/\partial S)_{P,N}$ shown in Figs. 2e and f, have asymptotes at densities just after the vapor spinodal and right before the liquid spinodal, and are positive in a region between the asymptotes. One of these thermodynamic relations has a clear physical interpretation:

$$\left(\frac{\partial T}{\partial S}\right)_{P,N} = \frac{T}{N\left(C_p^0 + C_p^{\text{r}}\right)}, \tag{29}$$

where the isobaric heat capacity, C_p, is split into an ideal gas contribution (superscript 0) and a residual contribution (superscript r). While C_p^{r} goes to $\pm\infty$ at the spinodals, C_p^0 is positive and depends only on the temperature. It is thus constant in Figs. 2 and 3. While $C_p^0(T)$ can be determined experimentally and is well-known for methane, $C_p^{\text{r}}(T,\rho)$ is unknown between the spinodals. The asymptotes of Eq. (29) correspond to the points where

$$C_p^{\text{r}}(T,\rho) = -C_p^0(T), \tag{30}$$

which can occur only between the spinodals. Interestingly, whether Eq. (30) is satisfied between the spinodals depends on which parameters that are used in the VdW EoS, and at which temperature the EoS is used. For instance, for methane at 92 K, Eq. (30) is clearly satisfied at two densities (see the asymptotes in Figs. 2e and f). However, for methane at 157 K, the same EoS predicts that $C_p^{\text{r}}(T,\rho) < -C_p^0(T)$ for all densities between the spinodals, where both of the thermodynamic relations in Eq. (18) remain negative between the spinodals, as shown in Fig. 3.

We shall next discuss if there are any physical arguments for why the thermodynamic quantities in Eqs. (16–18) should remain negative between the spinodals. To examine thermodynamic stability, we evaluate the sign of the eigenvalues of the Hessian matrices, since they define whether a stationary point of the energy state function is a minimum (only positive eigenvalues), a

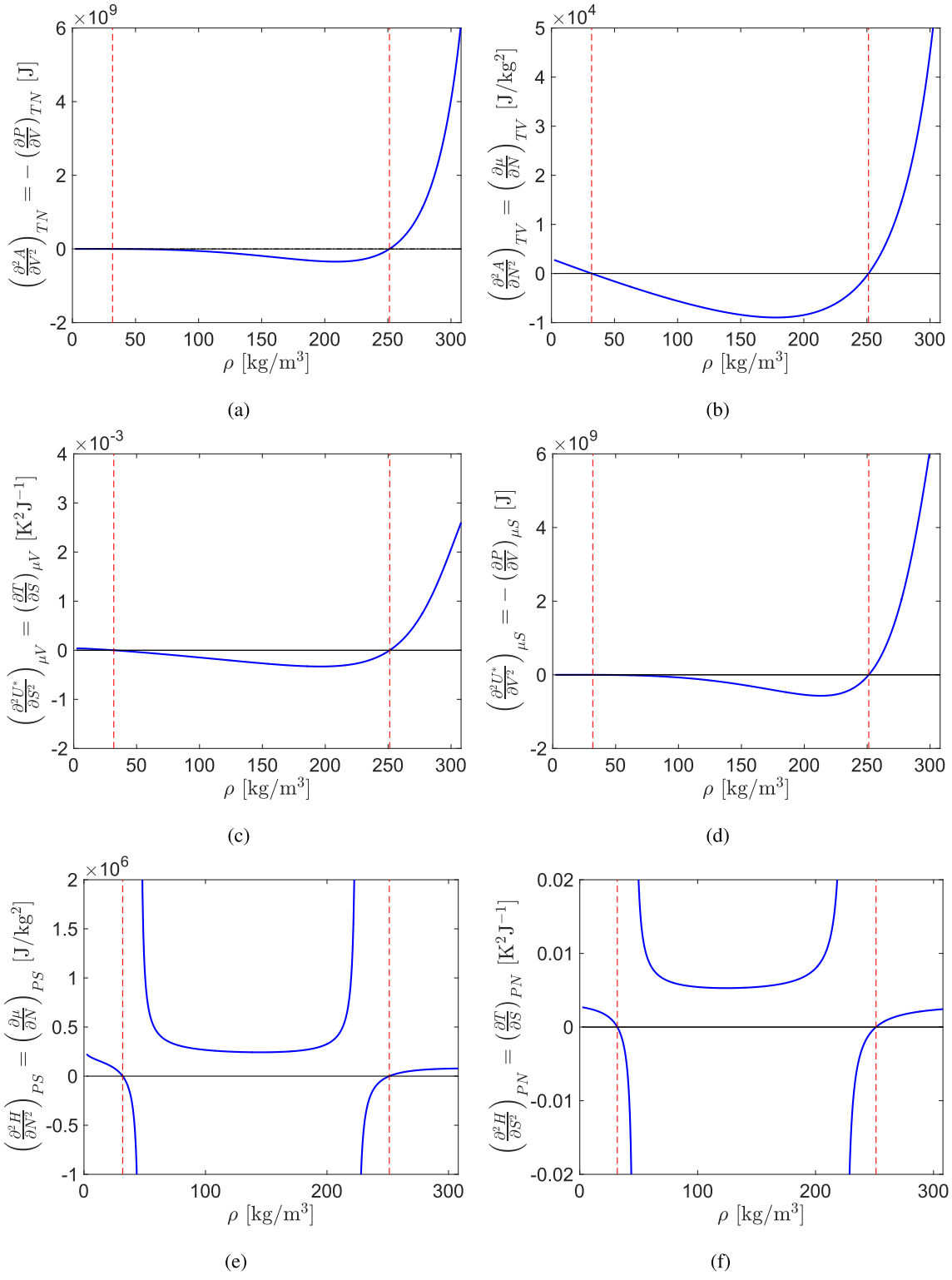

Fig. 2. A plot of Eqs. (16–18) through the two-phase region in the case of methane at 92 K as predicted by the Van der Waals cubic EoS (blue solid lines). The vertical red dashed lines show where the quantities pass through zero. The reported values are for 1 kmol of fluid. (For interpretation of the references to colour in this figure legend, the reader is referred to the web version of this article.)

maximum (only negative eigenvalues) or a saddle point (positive and negative eigenvalues).

First, let us discuss the rank of Hessian matrices and hence how many non-zero eigenvalues we expect. Since the energy state functions are Euler homogeneous functions of first degree in their extensive variables, the highest possible rank of their Hessian matrices is $r - 1$, where r is the number of extensive variables (we refer to Sec. 1.3 in Ref. [41] for details). Thus, for all the Hessian matrices, we expect at least one eigenvalue to be zero since they are singular [41]. For a single-component fluid, this gives a maximum

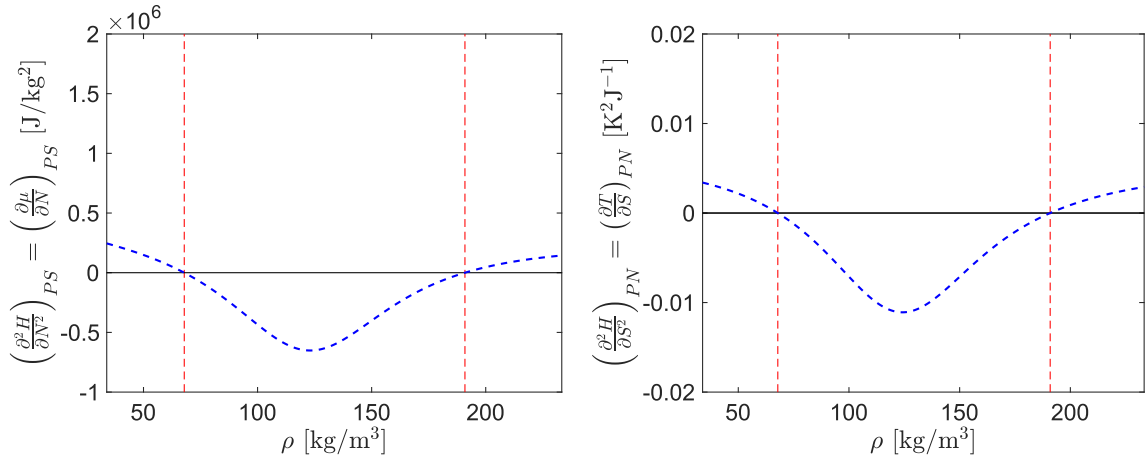

Fig. 3. A plot of two of the thermodynamic relations in Eq (18) through the two-phase region in the case of methane at 157 K as predicted by the VdW EoS (blue dashed lines). The vertical red dashed lines show where the quantities pass through zero. The reported values are for 1 kmol^3 of fluid. (For interpretation of the references to colour in this figure legend, the reader is referred to the web version of this article.)

of two non-zero eigenvalues for U and one non-zero eigenvalue for U^*, H and A. We have plotted the non-zero eigenvalues in Fig. 4 for methane, as described by the VdW EoS at 92 K (solid lines). In the figure, the eigenvalues have been divided by the eigenvalue of the liquid phase at saturation, and the subscripts refer to which energy state function the eigenvalues come from.

Fig. 4 shows that except for one of the eigenvalues of the Hessian matrix of U, $\lambda_{U,1}$, all eigenvalues go from positive to negative at the spinodals. This means that the internal energy goes from being a *local* minimum to a saddle point at the spinodals (one positive and one negative eigenvalue), while U^*, H and A go from local minima to maxima at the spinodals. Except for the eigenvalue of the Hessian matrix of the enthalpy displayed in Fig. 4c, the eigenvalues look very similar at 157 K and have not been plotted.

The asymptotes in the diagonal elements of the Hessian matrix of H at 92 K displayed in Fig. 2e and f are also reflected in asymptotes at the same densities in λ_H. In fact, Fig. 4c shows that the eigenvalue of $\nabla_{S,N}\nabla_{S,N}$ H goes from negative to positive in a region between the spinodals. When the asymptotes in the diagonal elements of the Hessian matrix of H disappear, such as at 157 K (see Fig. 3), then λ_H remains negative between the spinodals, similar to $\lambda_{U,2}$, λ_{U^*} and λ_A, as shown by the blue dashed lines in Fig. 4d.

Since all eigenvalues of the Hessian matrix of the enthalpy are non-negative in a region between the spinodals, the energy state function is a minimum. The VdW EoS thus predicts a uniform phase between the spinodals to be "pseudo-stable" in an adiabatic system kept at constant pressure, since the enthalpy is then the appropriate energy state function to examine.

In a macroscopic, single-phase system of arbitrary size, the thermodynamic stability of a sub-volume within the fluid should be independent of the choice of surroundings. Moreover, a pseudo-stable phase has never been observed experimentally between the spinodals, regardless of which experimental conditions that have been chosen. Therefore, the positive value of λ_H between the spinodals is an artifact of the VdW EoS and its parameters. We find a similar behavior of other cubic EoS, such as SRK and PR, where λ_H becomes positive between the spinodals at low temperatures. This is surprising, as its shows that even cubic EoS that have been considered to have a "physically admissible" behavior between the spinodals exhibit inconsistencies in the unstable domain of the single-phase fluid. To summarize: If one can find a state between the spinodals where, for any choice of energy state function, all eigenvalues of the Hessian are positive (one eigenvalue is always zero), one has found a pseudo-stable phase in that region. On the contrary, if at least one eigenvalue stays negative, such states are thermodynamically unstable. Thus, if we assume that such states are physically inadmissible, we arrive at the following statement:

> A sufficient condition for EoS to avoid inadmissible pseudo-stable states between the vapor and liquid spinodals is that at least one eigenvalue of the Hessian of the energy state function goes from positive to negative at, and remains negative between, the spinodals, for any choice of energy state function.

Fig. 2 shows that even if the EoS exhibits a physically admissible behavior for many of the state functions, this does not guarantee a physically admissible behavior for all energy state functions, unlike what is suggested in the work by Elhassan and coauthors [48]. We can also make some statements about the suitability of using Eqs. (16–18) as inequality constraints in fitting an EoS for a single-component fluid (similar statements can be made about multi-component fluids).

We know the following about the Hessian matrices of the energy state functions: They are singular, meaning that one of the eigenvalues is always zero and they are symmetric. Since the sum of the eigenvalues of a matrix equals the sum of the diagonal elements, one can prove mathematically that the two thermodynamic quantities in each of Eqs. (16–18) will always have the same sign for a single-component fluid. Therefore, it is only necessary to use one thermodynamic relation in each of the pairs in Eqs. (16–18) as an inequality constraint between the spinodals, where they have to be negative for a physically admissible behavior in the unstable region of the single-component fluid.

3.3. The spinodals and the limit of homogeneous nucleation

In Sec. 3.1 we argue that it is important to determine the spinodal precisely to arrive at EoS that are accurate in the metastable domain. In what follows, we investigate to which extent the EoS that are available today differ in their predictions of the spinodal.

Solving phase equilibrium calculations has received much attention in the literature. This can be challenging, in particular for multicomponent mixtures and multiparameter EoS [49]. Determining the spinodal has a comparable degree of complexity to phase equilibrium calculations, where a set of algebraic equations have to be solved based on the underlying EoS. However, robust

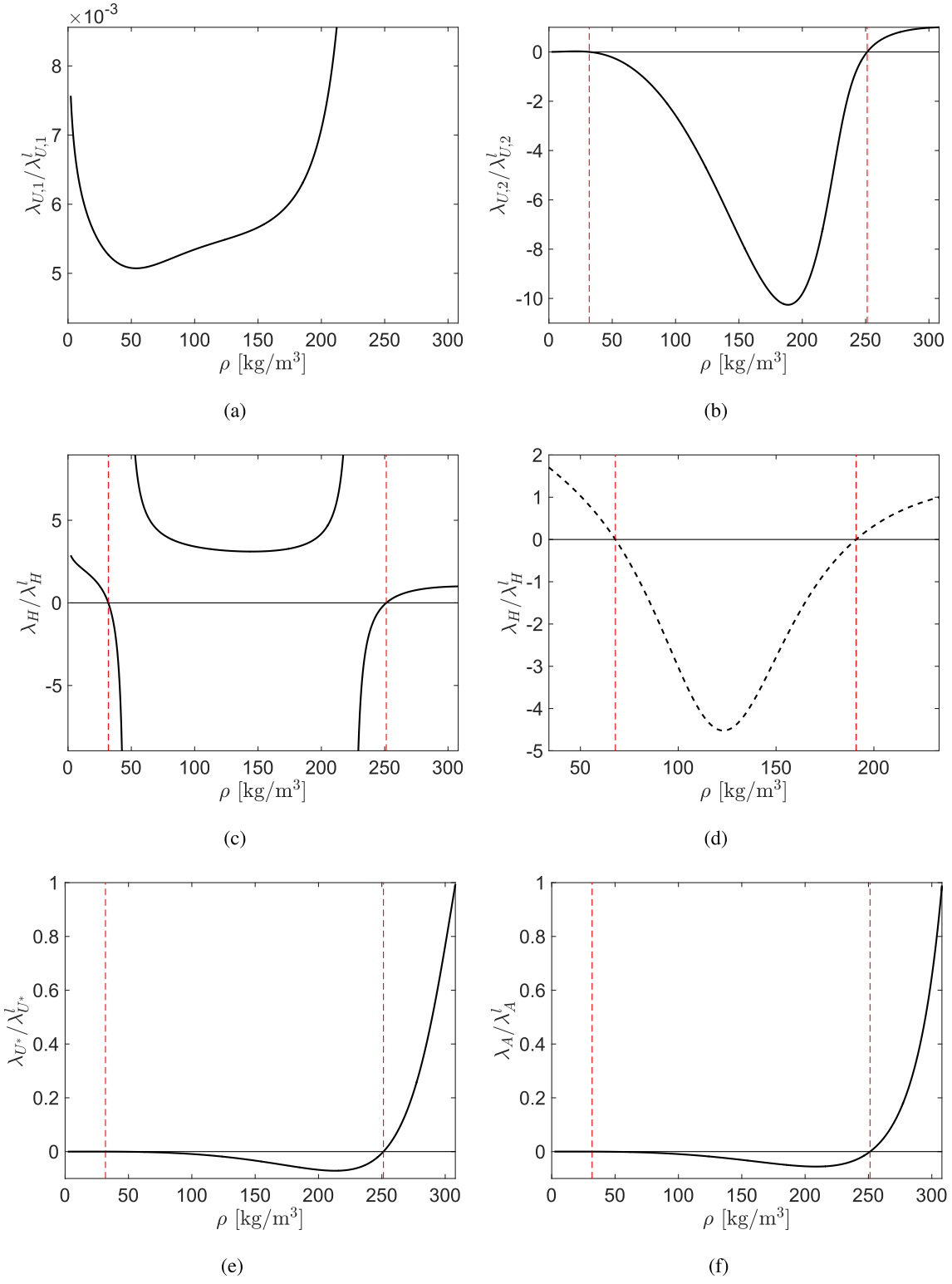

Fig. 4. A plot of the normalized eigenvalues of the energy state functions through the two-phase region in the case of methane at 92 K as predicted by the Van der Waals cubic EoS (black solid lines). The dashed line represents the eigenvalue the Hessian matrix of the enthalpy at 157 K. The vertical red dashed lines show where the quantities pass through zero. (For interpretation of the references to colour in this figure legend, the reader is referred to the web version of this article.)

and accurate methods for obtaining the spinodal have received far less attention in the literature than phase equilibrium calculations, partly due to the spinodal being less needed in engineering calculations. Previous work on the topic has mainly been limited to simple cubic EoS and pure substances [9,20–24].

In Fig. 5 we have used the methodology described in Sec. 2.2.3 to obtain the spinodal curve of a multicomponent natural gas mixture with one of the most accurate EoS available today, GERG2008 [50].

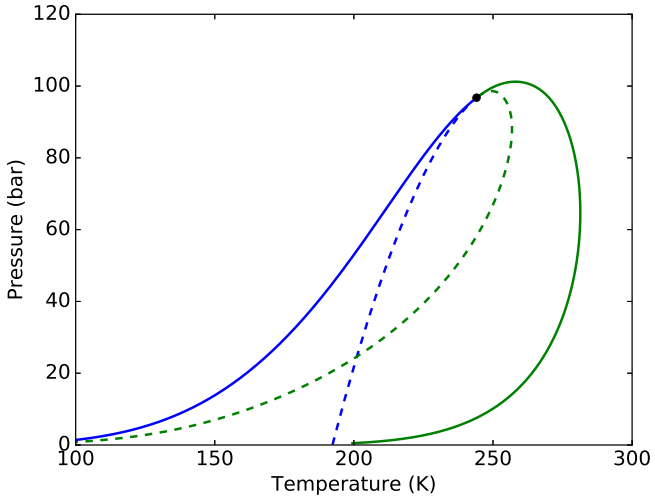

Fig. 5. Illustration of the phase envelope and spinodal curves obtained with the GERG2008 EoS for a five-component mixture of methane (75 mol-%), ethane (10 mol-%), propane (7 mol-%), butane (3 mol-%) and nitrogen (5 mol-%). The bubble line (solid blue), the dew line (solid green), the liquid spinodal (dashed blue) and the gas spinodal (dashed green) all meet in the critical point (black dot). (For interpretation of the references to colour in this figure legend, the reader is referred to the web version of this article.)

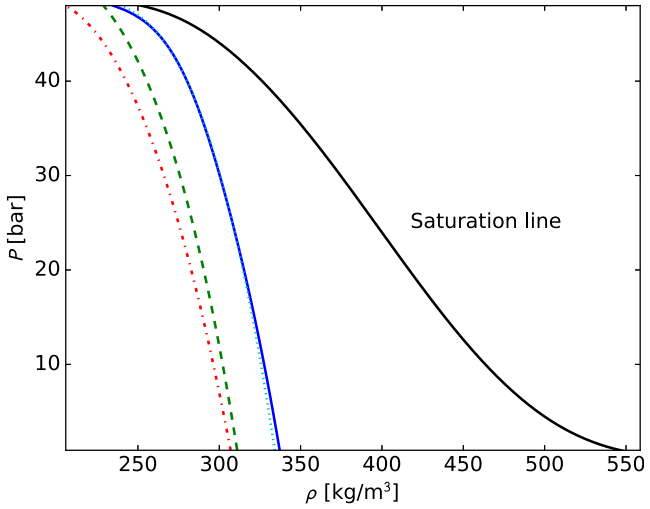

Fig. 6. The liquid density and pressure at the liquid spinodal curve for ethane, calculated using GERG2008 (solid blue), PC-SAFT (dashed green), PR (dash-dot red) and extended CSP (dotted cyan). The saturation line is given by the solid black line. (For interpretation of the references to colour in this figure legend, the reader is referred to the web version of this article.)

The figure demonstrates that the method we have presented is robust, even in the vicinity of the critical point, scalable to multi-component mixtures and applicable to complex non-analytical EoS. We observe, from a comparison of the solid and the dashed lines in Fig. 5, that there is a significant distance in the *TP* -space between the coexistence limits (solid lines) and the spinodal curves (dashed lines).

In what follows, we discuss the predicted spinodal for hydrocarbons with a selection of EoS representative of what is used in modern applications. Herein, we mainly focus on the pressure and temperature. In this discussion it is however crucial to recognize that the liquid density can change dramatically within the metastable region, even though it might only span a few degrees kelvin. An illustrative example of this is given in Fig. 6, showing the density and pressure of the liquid spinodal of ethane compared to the saturation line. At low pressures, the liquid density of the metastable fluid near the spinodal curve can be half of that at the saturation curve. Moreover, the difference in liquid density at the spinodal for different EoS can also be significant.

Fig. 7 shows the spinodal curve in the *TP* -space compared to the corresponding homogeneous nucleation limit and available experimental data for the limit of superheat for a selection of pure species. For all three substances considered here, there is a clear agreement between the limit of superheat predicted by nucleation theory and experimental data obtained from the droplet explosion method. Table 1 shows the absolute average deviation (AAD) of the experimental data points relative to the limit of superheat from classic nucleation theory for pure components and binary mixtures. The overall AAD between the predictions from CNT and the experimental measurements for the limit of superheat is only 1.0 K for pure species and 2.4 K for mixtures. Thus, even though CNT does not accurately predict the exact nucleation rates of fluids [1], it accurately reproduces the superheat limit.

The gap between the limit of superheat predicted by CNT and the liquid spinodal curve thus accurately represents the experimentally unobtainable part of the metastable region, caused by thermal fluctuations in the liquid. Overall, the liquid spinodal curves predicted using GERG2008, PC-SAFT, PR, and CSP agree within 2–3 K in the range from atmospheric to critical pressure. A notable exception is the liquid and vapor spinodals for n-pentane calculated using the PC-SAFT EoS (Fig. 7b). Here, a significant inaccuracy in the predicted critical point seems to offset the entire liquid spinodal curve by 5–10 K. This suggests that it is imperative for the EoS to reproduce the critical point of the fluid to provide reliable predictions of the spinodal. Note that while the CNT predictions depend on an estimated liquid density, surface tension, as well as the value of J_{crit}, a sensitivity analysis showed that the predicted limit of superheat matched experimental data for reasonable perturbations of ρ and σ, and for J_{crit} differing by orders of magnitude.

For the vapor spinodal there is a significantly larger span in the predicted spinodal curves from the four EoS than for the liquid spinodal. In particular, at a pressure of 0.9 bar, the difference in the vapor spinodal ranges from 42.4–85.1 K for methane, 135.5–213.6 K for n–pentane and 32.6–59.7 K for nitrogen. Table 2 shows the pressure-averaged standard deviation (with regard to EoS) in kelvin for a number of light hydrocarbons and nitrogen. The spread in predictions is higher for the vapor spinodal than the liquid spinodal, with an average standard deviation of 6.29 K for the former.

Fig. 8 shows the binary mixture liquid and vapor spinodal temperature at atmospheric pressure for the GERG2008, PC-SAFT, PR and extended CSP EoS, as a function of the second component mole fraction. The spinodal curves are compared to the bubble and dew lines, the superheat and supersaturation limits predicted by CNT, as well as available experimental data for the limit of superheat. Again, there is a good agreement between liquid superheat limit obtained in droplet explosion experiments and the limit predicted by classic nucleation theory. The predicted liquid spinodals mostly agree within 5 K. Moreover, the results indicate that for these species, a mole-weighted average of pure specie spinodal can provide an accurate estimate of the mixture spinodal.

The binary mixture vapor spinodals (Fig. 8, right) demonstrates a larger internal spread than what is the case for the liquid spinodal curves. Specifically, for an even mixture, the vapor spinodal temperature ranges from 85.9–154.7 K for ethane/propane, 108.9–177.0 K for propane/n–butane and 154.4–227.3 K for n–pentane/n–hexane. This behavior is consistent with what was

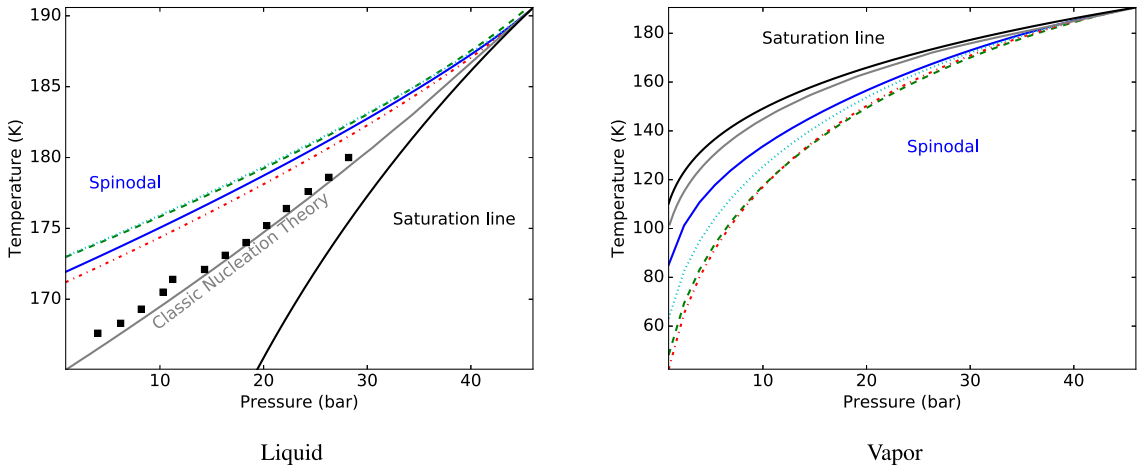

(a) Methane

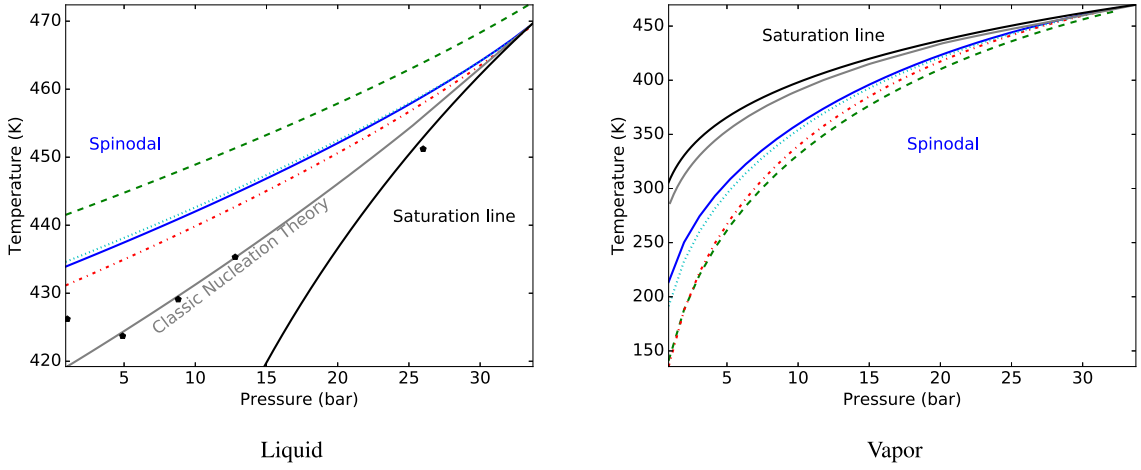

(b) n-Pentane

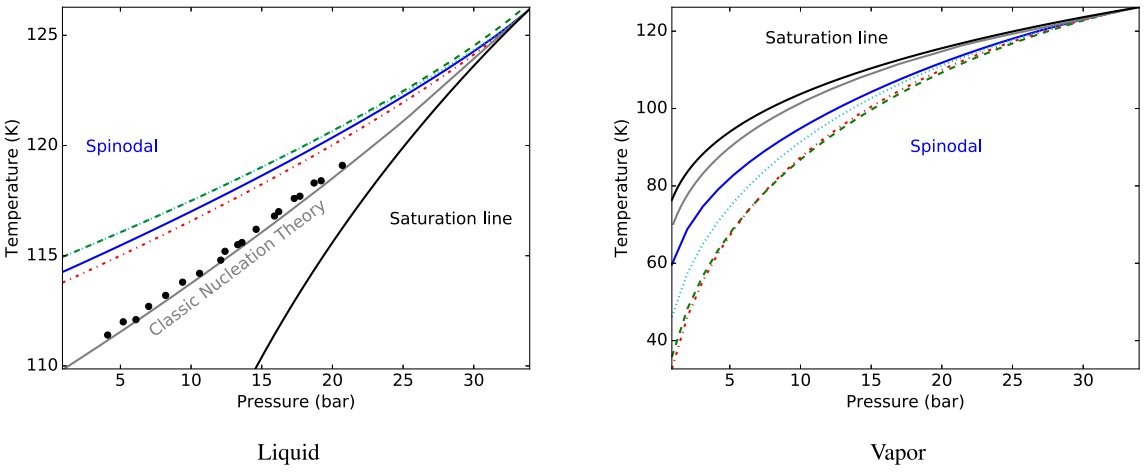

(c) Nitrogen

Fig. 7. Comparison of pure-component spinodal curves (liquid and vapor), superheat and subcool limits predicted using CNT (solid gray) and saturation line (solid black). The saturation lines are calculated with GERG2008. Spinodal curves are shown for four different EoS: GERG2008 (solid blue), PC-SAFT (dashed green), PR (dash-dot red) and extended CSP (dotted cyan). Experimental data from various studies of the limit of superheat are also shown: methane by Baidakov and Skripov [51] (squares), n-pentane compiled by Avedisian [8] (pentagons), nitrogen by Baidakov and Skripov [51] (circles). (For interpretation of the references to colour in this figure legend, the reader is referred to the web version of this article.)

Table 1
The average absolute deviation (AAD) in the temperature for the experimental data for the limit of superheat compared to classic nucleation theory for pure components and mixtures at pressure ranging from 0.9 bar to the critical pressure.

	AAD (K)
Methane	0.62
n-Pentane	0.28
Nitrogen	2.21
Ethane/Propane	4.5
Propane/n-Butane	1.2
n-Pentane/n-Hexane	1.6

Table 2
The standard deviation in the temperature with regard to EoS for the predicted spinodal. For the GERG2008, PC-SAFT, PR, and CSP EoS. Standard deviations are averaged for pressures ranging from 0.9 bar to the critical pressure.

	Liquid (K)	Vapor (K)
Methane	0.44	4.07
Ethane	1.13	6.62
Propane	1.60	7.15
n-Butane	2.19	7.99
n-Pentane	2.86	9.31
Nitrogen	0.30	2.61
Overall	1.42	6.29

observed for pure species (Fig. 7 right). The highest predictions for the vapor spinodal all come from the multiparameter GERG2008 equation, while the lowest come from the simple cubic Peng–Robinson EoS. This further illustrates the inconsistency of widely used EoS when used in the metastable domain. Table 3 shows the average (over mole fractions) standard deviation (with regard to EoS) of the predicted liquid and vapor spinodal temperatures for mixtures. Again, as for pure species, the spread in predicted spinodal temperatures is significant, especially for the vapor spinodal.

3.4. How close to the spinodals can experiments bring us?

We showed in Sec. 3.3 that the limit of superheat from experiments agreed very well with predictions from CNT, both for single-component liquids (Fig. 7) and mixtures (Fig. 8). This does not contradict that CNT is unable to reproduce experimental nucleation rates, since the limit of superheat is insensitive to the exact choice of the critical nucleation rate in Eq. (27). We can therefore use CNT to estimate the limits for how close to the spinodal it is possible to get experimentally before homogeneous nucleation occurs spontaneously. In Fig. 9, we have used methane as example and plotted the phase envelope that encloses the two-phase region (blue solid line), the limit of homogeneous nucleation as predicted by CNT (green dashed line) and the spinodals (red solid line). The spinodals, the coexistence line and the homogeneous nucleation limit all merge in the critical point.

In the following, we shall refer to the function $P = P(T, \rho)$ as the thermodynamic surface of methane. Fig. 9 shows that:

1 On a curve on the thermodynamic surface that goes from the spinodal to the coexistence limit, the distance between the spinodal and the nucleation limit relative to the corresponding distance to the coexistence limit is significant.
2 The relative distance on this curve is much larger for metastable vapor than for metastable liquid.

Point number 1 means that there is large part of the thermodynamic surface where the properties of the metastable fluid are currently experimentally unavailable, in particular for metastable vapor. In the literature, some suggestions have been put forward on how to enter the region of the thermodynamic surface that is currently experimentally unavailable.

A recent work [56] shows how small closed containers can be used to completely prevent nucleation, achieving infinitely long-lived metastable states, referred to as superstable. Experiments can be carried out in quartz inclusions, similar to Ref. [6], where speed of sound measurements in the inclusion give information about the slope of $P(\rho)$ at constant entropy, similar to Ref. [57]. Since such experiments are very challenging, the perhaps most available methodology to study the properties of highly metastable states is to use molecular dynamics simulations in the canonical ensemble. For many fluids like alkanes, carbon dioxide and nitrogen, force fields have been developed that reproduce the thermodynamic properties from experiments very accurately [58]. Molecular Dynamics simulations are then capable of generating pseudo-experimental data in the metastable regions, or to estimate the spinodals of the fluid. Eventually, hybrid data sets with both experimental data and data from computations can be exploited in the fitting of the next generation multiparameter EoS, following a procedure similar to Rutkai et al. [59]. This represents a largely unexplored research topic for the future.

Bullet point 2 agrees with the results in Figs. 7 and 8, and shows that CNT predicts the nucleation limit to be closer to the spinodal for liquids than for vapor.

4. Conclusion

In this work, we have presented a method that can be used to obtain the thermodynamic stability limit of a single-phase fluid, called the spinodal. We demonstrated that the method was robust in vicinity of the critical point, scalable to multicomponent mixtures and applicable to complex non-analytical EoS.

We next discussed the role of the spinodal, the metastable and the unstable regions of the phase diagram of the single-phase fluid in the development of modern equations of state (EoS). Since the spinodal provides a reference for an extrapolation into the metastable domain from the saturation curve, and since much is known about the thermodynamic properties of the fluid at the spinodal, information about the spinodal can be used to characterize the properties or to estimate the uncertainty of the properties of fluids in the metastable domain.

A future goal should be to develop EoS without inadmissible pseudo-stable states in the unstable domain. This is of importance, both for combining them with mass based density functional theory and to develop thermodynamically consistent mixing rules with a physical interpretation. We proposed and evaluated a set of inequality constraints that can be used for this purpose in the fitting of modern EoS for single-component fluids.

We showed that there were large inconsistencies in predicted spinodals from a wide range of EoS such as cubic EoS, extended corresponding state EoS, SAFT and multiparameter EoS. The overall standard deviation in the prediction of the spinodal temperatures were 1.4 K and 2.7 K for single- and multi-component liquid-spinodals and 6.3 K and 26.9 K for single- and multi-component vapor spinodals. However, the range between the smallest and the largest predictions were significantly larger. For example, for an even mixture of hydrocarbons, the vapor spinodal temperature ranged from 85.9–154.7 K for ethane/propane, 108.9–177.0 K for propane/n–butane and 154.4–227.3 K for n–pentane/n–hexane. In general, there was a much larger spread in the prediction of the vapor-spinodal than the liquid-spinodal.

We also discussed the relationship between the measurable limit of superheat or supersaturation and the theoretical concept of

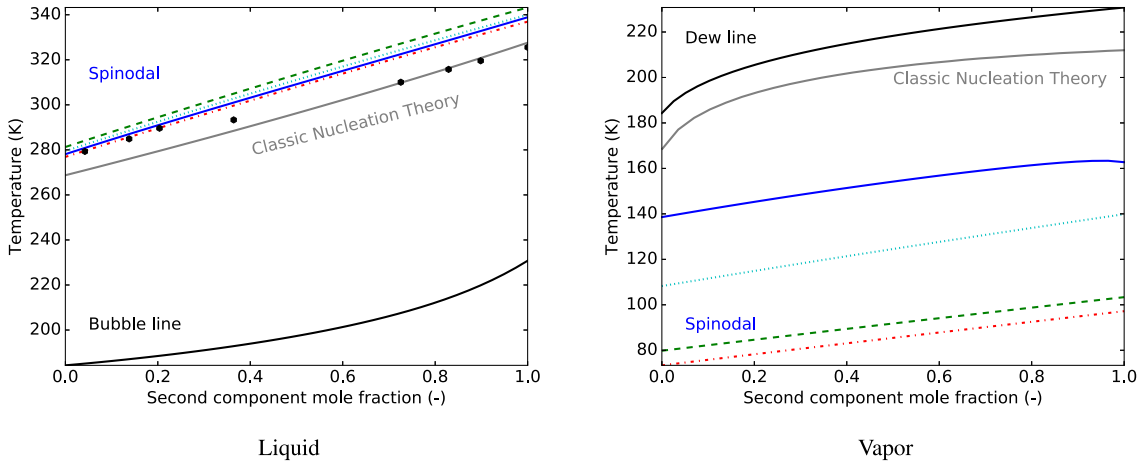

(a) Ethane + Propane

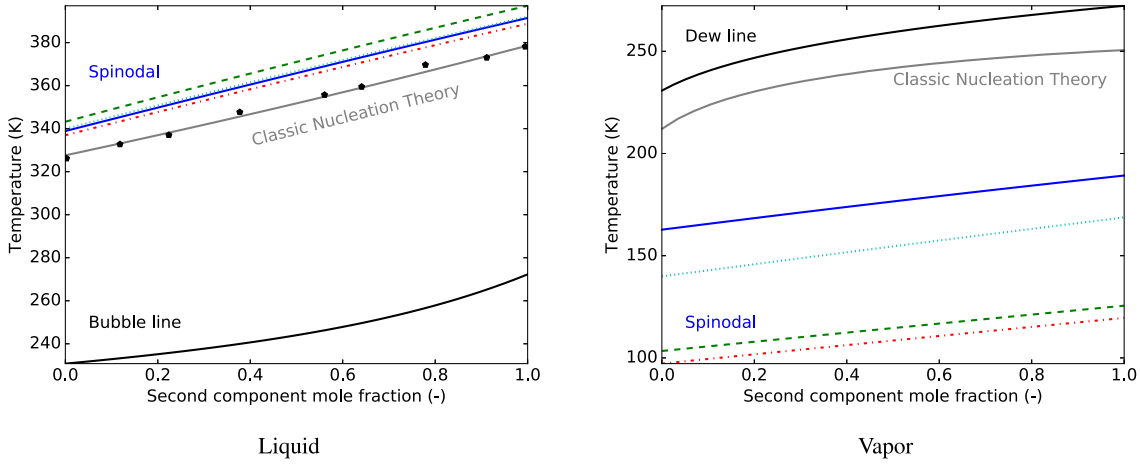

(b) Propane + n-Butane

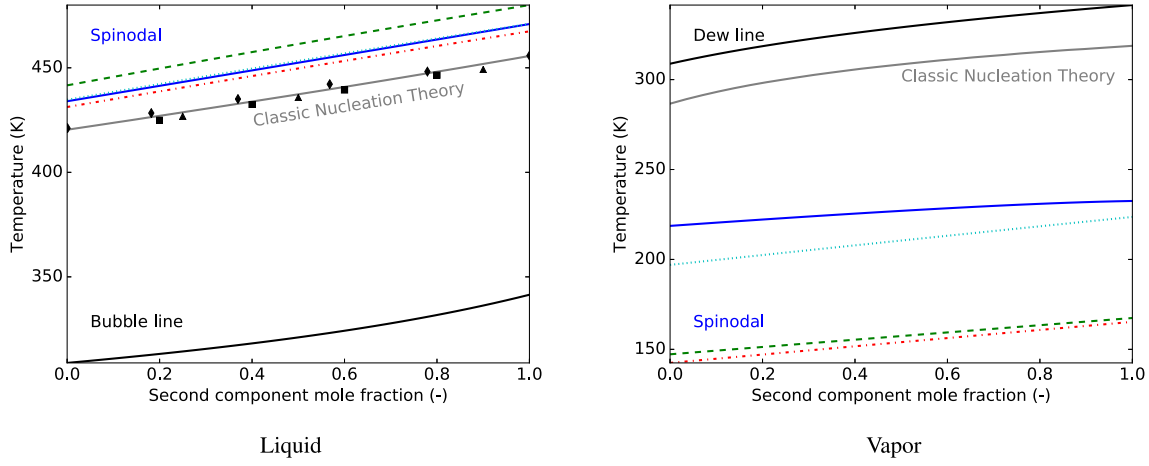

(c) n-Pentane + n-Hexane

Fig. 8. Comparison of the spinodal curve (liquid and vapor), superheat and subcool limits predicted using CNT (solid gray), and bubble and dew lines (solid black) for some binary mixtures at 1 bar. The bubble and dew lines are computed using GERG2008. Spinodals are shown for four different EoS: GERG2008 (solid blue), PC-SAFT (dashed green), PR (dash-dot red) and extended CSP (dotted cyan). Experimental data from various studies of the limit of superheat are also shown: ethane + propane by Porteous and Blander [52] (hexagons), propane + n-butane by Renner et al. [53] (pentagons), n-pentane + n-hexane by Holden and Katz [54] (squares), Park et al. [24] (diamonds) and Skripov [55] (triangles). (For interpretation of the references to colour in this figure legend, the reader is referred to the web version of this article.)

Table 3
The standard deviation in the temperature for the predicted spinodal limit for binary mixtures at atmospheric pressure using the GERG2008, PC-SAFT, PR, and CSP EoS. Standard deviations are averaged over all mole fractions.

	Liquid (K)	Vapor (K)
Methane/Ethane	1.85	21.51
Methane/Propane	2.62	23.34
Ethane/Propane	2.05	27.22
Ethane/n-Butane	2.67	28.92
Propane/n-Butane	2.70	28.13
n-Pentane/n-Hexane	4.31	31.97
Overall	2.70	26.85

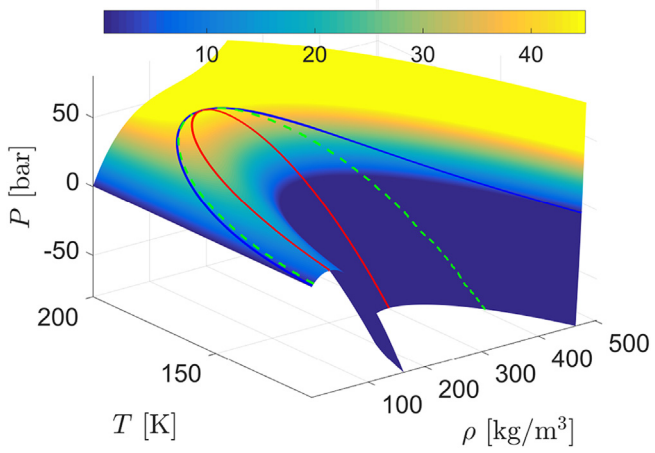

Fig. 9. A three-dimensional representation of the thermodynamic landscape of methane (relation between P, T and ρ) as predicted by the PR EoS. Here, the blue solid line encloses the two-phase region, the green dashed lines denote the states where Eq. (27) is satisfied and the homogeneous nucleation rate as predicted by CNT is so fast that the single-phase fluid appearers to decompose spontaneously into two phases. The red solid lines denote the spinodal, and enclose a region in which the single-phase fluid is unstable. (For interpretation of the references to colour in this figure legend, the reader is referred to the web version of this article.)

the spinodal. While nucleation rates from CNT can deviate orders of magnitude from experiments, we found that the limit of superheat experiments agreed within 1.0 K and 2.4 K with predictions from CNT for single- and multi-component fluids respectively.

At present, a large part of the metastable domain of the phase diagram is experimentally unavailable, in particular for metastable vapor. Novel techniques, with experimental or computational methods, should be developed to characterize the thermodynamic properties in these regions, and to identify the thermodynamic states that define the spinodal.

Acknowledgment

The authors acknowledge the support from the Research Council of Norway (project number 244076). The authors thank “The Gas Technology Centre NTNU-SINTEF” for the support.

References

[1] P.G. Debenedetti, Metastable Liquids: Concepts and Principles, Princeton University Press, Princeton, 1996.
[2] F. Caupin, E. Herbert, Cavitation in water: a review, Comptes Rendus Phys. 7 (9) (2006) 1000–1017, http://dx.doi.org/10.1016/j.crhy.2006.10.015.
[3] K. Davitt, A. Arvengas, F. Caupin, Water at the cavitation limit: density of the metastable liquid and size of the critical bubble, Europhys. Lett. 90 (2010) 16002, http://dx.doi.org/10.1209/0295-5075/90/16002.
[4] F. Caupin, A. Arvengas, K. Davitt, M. El Mekki Azouzi, K.I. Shmulovich, C. Ramboz, D.A. Sessoms, A.D. Stroock, Exploring water and other liquids at negative pressure, J. Phys. Condens. Matter 24 (28) (2012) 284110, http://dx.doi.org/10.1088/0953-8984/24/28/284110.
[5] Q. Zheng, D.J. Durben, G.H. Wolf, C.A. Angell, Liquids at large negative pressures: water at the homogeneous nucleation limit, Science 254 (5033) (1991) 829–832, http://dx.doi.org/10.1126/science.254.5033.829.
[6] M. El Mekki Azouzi, C. Ramboz, J.F. Lenain, F. Caupin, A coherent picture of water at extreme negative pressure, Nat. Phyics 9 (2013) 38–41, http://dx.doi.org/10.1038/nphys2475.
[7] A. C. Hack, A. B. Thompson, Density and viscosity of hydrous magmas and related fluids and their role in subduction zone processes, J. Petrology 52 (1333–1362). doi:10.1093/petrology/egq048.
[8] C. Avedisian, The homogeneous nucleation limits of liquids, J. Phys. Chem. Reference Data 14 (3) (1985) 695–729, http://dx.doi.org/10.1063/1.555734.
[9] J. Salla, M. Demichela, J. Casal, BLEVE: a new approach to the superheat limit temperature, J. Loss Prev. Process Industries 19 (6) (2006) 690–700, http://dx.doi.org/10.1016/j.jlp.2006.04.004.
[10] R. Bubbico, E. Salzano, Acoustic analysis of blast waves produced by rapid phase transition of LNG released on water, Saf. Sci. 47 (4) (2009) 515–521, http://dx.doi.org/10.1016/j.ssci.2008.07.033.
[11] R.K. Eckhoff, Boiling liquid expanding vapour explosions (BLEVEs): a brief review, J. Loss Prev. Process Industries 32 (2014) 30–43, http://dx.doi.org/10.1016/j.jlp.2014.06.008.
[12] H. Vehkamäki, Classical Nucleation Theory in Multicomponent Systems, Springer Verlag, Berlin, 2006.
[13] A. Obeidat, J.S. Li, G. Wilemski, Nucleation rates of water and heavy water using equations of state, J. Chem. Phys. 121 (19) (2004) 9510–9516, http://dx.doi.org/10.1063/1.1806400.
[14] A. Obeidat, G. Wilemski, Gradient theory of nucleation in polar fluids, Atmos. Res. 82 (2006) 481–488, http://dx.doi.org/10.1016/j.atmosres.2006.02.005.
[15] W. Wagner, A. Pruß, The IAPWS formulation 1995 for the thermodynamic properties of ordinary water substance for general and scientific use, J. Phys. Chem. Reference Data 31 (2002) 387–535, http://dx.doi.org/10.1063/1.1461829.
[16] Ø. Wilhelmsen, A. Aasen, G. Skaugen, P. Aursand, A. Austegard, E. Aursand, M.Aa. Gjennestad, H. Lund, G. Linga, M. Hammer, Thermodynamic Modeling with Equations of State: present Challenges for Established Models, Under Revision.
[17] H. Wakeshima, K. Takata, On the limit of superheat, J. Phys. Soc. Jpn. 13 (11) (1958) 1398–1403, http://dx.doi.org/10.1143/JPSJ.13.1398.
[18] G.R. Moore, Vaporization of superheated drops in liquids, AIChE J. 5 (4) (1959) 458–466, http://dx.doi.org/10.1002/aic.690050412.
[19] J.H. Lienhard, A. Karimi, Homogeneous nucleation and the spinodal line, J. Heat Transf. 103 (1981) 61–64, http://dx.doi.org/10.1115/1.3244431.
[20] J.H. Lienhard, N. Shamsundar, P.O. Biney, Spinodal lines and equations of state: a review, Nucl. Eng. Des. 95 (1986) 297–314, http://dx.doi.org/10.1016/0029-5493(86)90056-7.
[21] N. Shamsundar, J.H. Lienhard, Equations of state and spinodal lines – a review, Nucl. Eng. Des. 141 (1) (1993) 269–287, http://dx.doi.org/10.1016/0029-5493(93)90106-J.
[22] P.O. Biney, W.-G. Dong, J.H. Lienhard, Use of a cubic equation to predict surface tension and spinodal limits, J. Heat Transf. 108 (2) (1986) 405–410, http://dx.doi.org/10.1115/1.3246938.
[23] C. Liu, D. Zeng, K. Xing, Superheat limit of liquid mixtures, Proc. Symposium Energy Eng. 21st Century 1 (2000) 373–378.
[24] H.-C. Park, K.-T. Byun, H.-Y. Kwak, Explosive boiling of liquid droplets at their superheat limits, Chem. Eng. Sci. 60 (7) (2005) 1809–1821, http://dx.doi.org/10.1016/j.ces.2004.11.010.
[25] G. Soave, Equilibrium constants from a modified Redlich–Kwong equation of state, Chem. Eng. Sci. 27 (6) (1972) 1197–1203, http://dx.doi.org/10.1016/0009-2509(72)80096-4.
[26] D.-Y. Peng, D.B. Robinson, A new two-constant equation of state, Industrial Eng. Chem. Fundam. 15 (1) (1976) 59–64, http://dx.doi.org/10.1021/i160057a011.
[27] J. F. Ely, I. M. F. Marrucho, Equations of State for Fluid Mixtures, IUPAC, 2000, Ch. The Corresponding-states Principle, pp. 289–320.
[28] Ø. Wilhelmsen, G. Skaugen, O. Jørstad, H. Li, Evaluation of SPUNG and other equations of state for use in carbon capture and storage modelling, Energy Procedia 23 (2012) 236–245, http://dx.doi.org/10.1016/j.egypro.2012.06.024.
[29] M.L. Michelsen, J.M. Mollerup, Thermodynamic Models: Fundamentals and Computational Aspects, second ed., Tie-Line Publictions, Holte, Denmark, 2007.
[30] W.G. Chapman, K.E. Gubbins, G. Jackson, M. Radosz, SAFT: equation-of-state solution model for associating fluids, Fluid Phase Equilibria 52 (1989) 31–38, http://dx.doi.org/10.1016/0378-3812(89)80308-5.
[31] J. Gross, G. Sadowski, Perturbed-chain SAFT: an equation of state based on a perturbation theory for chain molecules, Industrial Eng. Chem. Res. 40 (4) (2001) 1244–1260, http://dx.doi.org/10.1021/ie0003887.
[32] U. Setzmann, W. Wagner, A new equation of state and tables of thermodynamic properties for methane covering the range from the melting line to 625 K at pressures up to 100 MPa, J. Phys. Chem. Reference Data 20 (6) (1991) 1061–1155, http://dx.doi.org/10.1063/1.555898.
[33] R. Span, W. Wagner, A new equation of state for carbon dioxide covering the fluid region from the triple-point temperature to 1100 K at pressures up to 800 MPa, J. Phys. Chem. Reference Data 25 (6) (1996) 1509–1596, http://

dx.doi.org/10.1063/1.555991.
[34] R. Span, E.W. Lemmon, R.T. Jacobsen, W. Wagner, A reference quality equation of state for nitrogen, Int. J. Thermophys. 19 (4) (1998) 1121–1132, http://dx.doi.org/10.1023/A:1022689625833.
[35] C. Tegeler, R. Span, W. Wagner, A new equation of state for argon covering the fluid region for temperatures from the melting line to 700 K at pressures up to 1000 MPa, J. Phys. Chem. Reference Data 28 (3) (1999) 779–850, http://dx.doi.org/10.1063/1.556037.
[36] J. Smukala, R. Span, W. Wagner, New equation of state for ethylene covering the fluid region for temperatures from the melting line to 450 K at pressures up to 300 MPa, J. Phys. Chem. Reference Data 29 (5) (2000) 1053–1121, http://dx.doi.org/10.1063/1.1329318.
[37] O. Kunz, W. Wagner, The GERG-2008 wide-range equation of state for natural gases and other mixtures: an expansion of GERG-2004, J. Chem. Eng. Data 57 (11) (2012) 3032–3091, http://dx.doi.org/10.1021/je300655b.
[38] H.B. Callen, Thermodynamics and an Introduction to Thermostatistics, second ed., Wiley, New York, 1985.
[39] J.W. Tester, M. Modell, Thermodynamics and its Applications, Prentice Hall PTR, New Jersey, 1996.
[40] B.L. Beegle, M. Modell, R.C. Reid, Thermodynamic stability criterion for pure substances and mixtures, AIChe J. 20 (1974) 1200–1206, http://dx.doi.org/10.1002/aic.690200621.
[41] E.H. Chimowitz, Introduction to Critical Phenomena in Fluids, Oxford University Press, New York, 2005.
[42] R.A. Heidemann, A.M. Khalil, The calculation of critical points, AIChE J. 26 (5) (1980) 769–779, http://dx.doi.org/10.1002/aic.690260510.
[43] M.L. Michelsen, Calculation of critical points and phase boundaries in the critical region, Fluid Phase Equilibria 16 (1) (1984) 57–76, http://dx.doi.org/10.1016/0378-3812(84)85021-9.
[44] Ø. Wilhelmsen, D. Reguera, Evaluation of finite-size effects in cavitation and droplet formation, J. Chem. Phys. 142 (2015) 064703, http://dx.doi.org/10.1063/1.4907367.
[45] R.C. Reid, J.M. Prausnitz, B.E. Poling, The Properties of Gases and Liquids, McGraw Hill Book Co., New York, NY, 1987.
[46] E.W. Lemmon, R.T. Jacobsen, A new functional form and new fitting techniques for equations of state with application to pentafluoroethane (HFC-125), J. Phys. Chem. Reference Data 34 (2005) 69–108, http://dx.doi.org/10.1063/1.1797813.
[47] E.W. Lemmon, M.O. McLinden, W. Wagner, Thermodynamic properties of propane. III. a reference equation of state for temperatures from the melting line to 650 K and pressures up to 1000 MPa, J. Phys. Chem. Reference Data 54 (2009) 3141–3180, http://dx.doi.org/10.1021/je900217v.
[48] A.E. Elhassan, R.J.B. Craven, K.M. de Reuck, The area method for pure fluids and an analysis of the two-phase region, Fluid Phase Equilibria 130 (1997) 167–187, http://dx.doi.org/10.1016/S0378-3812(96)03222-0.
[49] J. Gernert, A. Jäger, S. R, Calculation of phase equilibria for multi-component mixtures using highly accurate helmholtz energy equation of state, Fluid Phase Equilibria 375 (2014) 209–218, http://dx.doi.org/10.1016/j.fluid.2014.05.012.
[50] Software for the Reference Equation of State GERG-2008 for Natural Gases and Other Mixtures, 2016, http://www.thermo.rub.de/en/prof-w-wagner/software/gerg-2004-gerg-2008.html.
[51] V.G. Baidakov, V.P. Skripov, Superheating and surface tension of vapor nuclei in nitrogen, oxygen, and methane, Russ. J. Phys. Chem. 56 (1982) 499–501.
[52] W. Porteous, M. Blander, Limits of superheat and explosive boiling of light hydrocarbons, halocarbons, and hydrocarbon mixtures, AIChE J. 21 (3) (1975) 560–566, http://dx.doi.org/10.1002/aic.690210319.
[53] T.A. Renner, G.H. Kucera, M. Blander, Explosive boiling in light hydrocarbons and their mixtures, J. Colloid Interface Sci. 52 (2) (1975) 391–396, http://dx.doi.org/10.1016/0021-9797(75)90215-5.
[54] B.S. Holden, J.L. Katz, The homogeneous nucleation of bubbles in superheated binary liquid mixtures, AIChE J. 24 (2) (1978) 260–267, http://dx.doi.org/10.1002/aic.690240215.
[55] V.P. Skripov, Metastable Liquids, John Wiley & Sons, 1974.
[56] Ø. Wilhelmsen, D. Bedeaux, S. Kjelstrup, D. Reguera, Communication: superstabilization of fluids in nanocontainer, J. Chem. Phys. 141 (2014) 071103, http://dx.doi.org/10.1063/1.4893701.
[57] A.D. Alvarenga, M. Grimsditch, R.J. Bodnar, Elastic properties of water under negative pressures, J. Chem. Phys. 98 (1993) 8392–8396, http://dx.doi.org/10.1063/1.464497.
[58] J.J. Potoff, J. Ilja Siepmann, Vapor-liquid equilibria of mixtures containing alkanes, carbon dioxide, and nitrogen, AIChE J. 47 (2001) 1676–1682, http://dx.doi.org/10.1002/aic.690470719.
[59] G. Rutkai, M. Thol, R. Lustig, R. Span, J. Vrabec, Communication: fundamental equation of state correlation with hybrid data sets, J. Chem. Phys. 139 (2013) 041102, http://dx.doi.org/10.1063/1.4817203.